Journal of
Materials Chemistry A

Materials for energy and sustainability

Accepted Manuscript

This article can be cited before page numbers have been issued, to do this please use: H. He, H. Tong, X. Song, X. song and J. Liu, *J. Mater. Chem. A*, 2020, DOI: 10.1039/D0TA00748J.

ROYAL SOCIETY OF CHEMISTRY

rsc.li/materials-a

View Article Online
DOI: 10.1039/D0TA00748J

Highly Stable Zn Metal Anode Enabled by Atomic Layer Deposited Al_2O_3 Coating for Aqueous Zinc-ion Batteries

Huibing He,[a] Huan Tong,[b] Xueyang Song,[a] Xiping Song [b], Jian Liu [a,*]

[a] *School of Engineering, Faculty of Applied Science, The University of British Columbia, Kelowna, BC V1V 1V7 Canada*

[b] *State Key Laboratory for Advanced Metals and Materials, University of Science and Technology Beijing, Beijing 100083, PR China*

[*] Corresponding author: jian.liu@ubc.ca (Jian Liu).

Abstract

Rechargeable aqueous zinc-ion batteries (ZIBs) have attracted increasing attentions as an energy storage technology for large-scale applications, due to their high capacity (820 mAh g^{-1} and 5854 Ah L^{-1}), inherent high safety, and their low cost. However, the overall performance of ZIBs has been seriously hindered by the poor rechargeability of Zn anode, because of the dendrite growth, passivation, and hydrogen evolution problems associated with Zn anode. Herein, Al_2O_3 coating by atomic layer deposition (ALD) technique was developed to address the aforementioned problems and improve the rechargeability of Zn anode for ZIBs. By coating the Zn plate with ultrathin Al_2O_3 layer, the wettability of Zn was improved and corrosion was inhibited. As a result, the formation of Zn dendrite was effectively suppressed, with significantly improved lifetime in the Zn-Zn symmetric cells. With the optimized coating thickness of 100 cycles, $100Al_2O_3$@Zn symmetric cells shown a reduced overpotential (36.5 mV) and a prolonged life span (over 500 h) at 1 mA cm^{-2}. In addition, the $100Al_2O_3$@Zn has been verified in Zn-MnO_2 batteries using layered δ-MnO_2 as the cathodes and consequently superior electrochemical performance with a high capacity retention of 89.4% after over 1000 cycles at a current density of 1 mA cm^{-2} (3.33C for MnO_2) is demonstrated. It is expected that the novel design of Al_2O_3 modified Zn anode may pave the way towards high-performance aqueous ZIBs and shed light on development of other metal anode-based battery systems.

Keywords: zinc ion batteries, zinc metal anode, atomic layer deposition, Al_2O_3 coating, dendrite

View Article Online
DOI: 10.1039/D0TA00748J

1. Introduction

Nonaqueous lithium-ion batteries (LIBs) have dominated the global energy storage market over the past decades, due to their high energy density, high power density, and long cycle life.[1,2] However, the increasing concerns over limited lithium resources, high cost, and safety issues limit their future applications in large-scale energy storage.[3] Sodium-ion batteries (SIBs) and potassium-ion batteries (KIBs) have been developed as alternatives to LIBs, because of their relatively abundant sodium (or potassium) resources in the Earth's crust. However, they still suffer from low energy density, the use of highly toxic and flammable organic electrolytes, and the high manufacturing cost and safety issues.[4,5] The drawbacks of these nonaqueous-based systems motivate us to explore alternative battery chemistry with lower cost, higher safety, and longer cycle life.

Recently, aqueous zinc-ion batteries (ZIBs) have gained remarkable attentions as a promising energy storage technology, owing to the appealing advantages of Zn anode, including high theoretical capacity (820 mAh g^{-1}), low redox potential (−0.762 V vs. SHE), high abundance, and environmental benignity.[6-9] More importantly, the replacement of organic electrolytes with aqueous electrolytes is of great significance to achieve intrinsic safety, environmental protection, and cost saving. Additionally, aqueous electrolytes offer about 2 orders of magnitude higher ionic conductivity (~ 1 S cm^{-1}) than nonaqueous ones (~ 1−10 mS cm^{-1}).[10-16] However, the development of aqueous ZIBs is limited by the Zn anode, which suffers from dendrite growth, low efficiency, and poor cycle life.[17,18] The sharp and high-resistant Zn dendrites could not only lead to short circuit by penetrating the separator and sudden failure of ZIBs, but also cause rapid capacity decay by lowering efficiency and elevating internal resistance.[18,19]

To circumvent these problems resulting from Zn dendrites, various strategies have been proposed to stabilize Zn anode, including novel structure design,[20-22] Zn alloying,[23] surface modification,[24-30] conductive substrates[31-33] and electrolyte optimization[13,15,34]. Among these strategies, surface modification represents a facile and effective approach to tune the interaction between Zn anode and electrolyte. Metal nanoparticles,[24] organic polymers,[25,26] carbon-based materials[27-29] and metallic compounds,[30,40] have been investigated as protective layers on Zn-based electrodes, rendering better electrochemical performance. For example, Zhi's group reported that quasi-isolated nano-Au particles

View Article Online
DOI: 10.1039/D0TA00748J

on the Zn surface served as heterogeneous seeds for Zn deposition, and enabled stable Zn-plating/stripping process on the Zn anode.[24] These nano-Au particles with high curvature and large local electric field preferentially absorbed Zn^{2+} to uniformly nucleate and grow as Zn-flake-arrays, effectively suppressing the formation of big and uneven dendrites/protrusions. As a result, the Au-nanoparticle decorated Zn anode demonstrated excellent cycling stability with 2000 h in Zn|Zn symmetric cells and 2000 cycles in Zn-MnO_2 batteries. Cui and co-workers designed a polyamide coating layer on the Zn anode to elevate the nucleation barrier and restrict 2D diffusion of Zn^{2+}, which effectively regulated Zn deposition behavior in the aqueous electrolyte.[26] This polyamide coating served as a buffer layer that isolated active Zn from bulk electrolytes, and suppressed the corrosion induced by water and O_2. With this synergic effect, the polyamide-modified Zn anode exhibited 60-fold enhancement in lifetime (over 8,000 hours) compared to the bare Zn, even at a high areal capacity of 10 mAh cm^{-2} (10 mA cm^{-2} for 1 h, 85% depth of discharge). Wang et al.[28] obtained a spontaneously reduced graphene oxide coating on Zn foil (Zn/rGO) to promote uniform Zn electrodeposition and improve the cycling stability. This self-assembled, layered rGO on a Zn surface provided a large electroactive area and a soft substrate for Zn electrodeposition, which significantly mitigated Zn dendritic growth by eliminating its driving force. Compared with bare Zn, the Zn/rGO anode exhibited much lower overpotential (~20 mV at 1 mA cm^{-2}) and excellent long-life cyclability. Recently, Kang et al.[30] designed a porous nano-$CaCO_3$ coating as a protective layer to achieve a uniform and bottom-up Zn stripping/plating. This strategy effectively suppressed the development of Zn dendrites that may cause large polarization and internal short circuit, thus improving the Coulombic efficiency (CE) and cycling stability of Zn batteries. All these results suggest that surface modification as an efficient way can construct robust Zn anode, contributing to superior electrochemical performance during repeated Zn stripping/plating cycles.

Atomic layer deposition (ALD) is a promising thin film deposition technique that is capable of precisely controlling film thickness at the atomic level, owing to its self-limiting nature of the gas-solid reactions during the deposition process.[35] Over the past years, ALD has been extensively applied to deposit protection layers on anode and cathode materials to prevent direct exposure of the electrode to electrolyte, leading to improved electrochemical performance in lithium/sodium-based batteries.[37-40] The performance enhancement could be achieved using just a few nanometers of surface coatings by ALD,

View Article Online
DOI: 10.1039/D0TA00748J

therefore adding negligible weight to the electrode. Moreover, the ALD coating has great potential for industrial application through roll-to-roll or fluidized bed ALD process. However, the application of ALD in aqueous ZIBs is yet to be fully exploited. Recently, Mai's groupfirst applied ALD TiO_2 coating as a protective layer on Zn anode. The amorphous TiO_2 layer acted as a buffer layer between Zn anode and electrolyte and suppressed the hydrogen evolution and the formation of inactive reaction by-products, leading to enhanced electrochemical performance of ZIBs.[36] Nevertheless, the ALD deposition of TiO_2 employed $TiCl_4$ as a Ti precursor, which yielded HCl by-product during deposition and was not ideal for practical applications.[36] In contrast, ALD Al_2O_3 is the most widely used coating material in LIBs, due to its effectiveness among all available ALD materials and its well-established industrial deposition process. However, there is no report of using ALD Al_2O_3 on the Zn anode, to the best of our knowledge. Al_2O_3 coating has been previously synthesized onto Zn particles by a sol–gel method, and reported to be able to mitigate hydrogen evolution reaction and delay the corrosion of the Zn anode in alkaline electrolyte.[41] Despite the improved performance, the Al_2O_3 coating by sol–gel method was uneven and rough on Zn particles, affecting its function as a protection layer. So, it is expected to have a systematic study on the effect of uniform Al_2O_3 coating on the Zn anodes with nanometers thickness by ALD technique.

In this work, we demonstrated the use of an ultrathin protective Al_2O_3 coating layer by ALD on Zn anode to achieve dendrite-free Zn deposition and high-performance Zn-MnO_2 batteries. The effect of ALD Al_2O_3 thickness on the cycling of Zn|Zn cells was investigated in detail. It was found that Zn anode with Al_2O_3 coating deposited using 100 ALD cycles ($100Al_2O_3$@Zn) showed reduced overpotential (36.5 mV) and prolong cycling lifespan (over 500 h) at 1 mA cm^{-2} in Zn|Zn symmetrical cells. Furthermore, Zn–MnO_2 battery built with $100Al_2O_3$@Zn anode exhibited a high capacity retention of 89.4% after 1000 cycles at a current density of 1 mA cm^{-2} (3.33C for MnO_2). The improved electrochemical performance was ascribed to the robust Zn metal anode enabled by nanoscale Al_2O_3 coating, which not only improved the surface wettability but also enhance the corrosion resistance of Zn metal, thus less conductive dendrites formation is effectively suppressed. It is expected that this work will provide new insight in interfacial engineering for metal anode and in the fundamental understanding of interfacial phenomena for high performance metal-based batteries.

View Article Online
DOI: 10.1039/D0TA00748J

2. Experimental section

2.1 Materials Preparation

ALD Al_2O_3 coating on zinc foil: Before ALD coating, zinc foil (0.2 mm in thickness) was cut into small round plates (Φ = 14 mm), and cleaned by sonication sequentially in DI water and in alcohol for 15 minutes, followed by natural drying in the air. Al_2O_3 coating on the Zn round plates was performed at 100 °C by alternatively supplying trimethylaluminum (TMA) and H_2O into a commercial ALD reactor (GEMStar™ XT Atomic Layer Deposition System). Al_2O_3 coatings were deposited on the Zn plates by adjusting ALD cycles from 30, 60, 100 to 200, which were named as $30Al_2O_3$@Zn, $60Al_2O_3$@Zn, $100Al_2O_3$@Zn, and $200Al_2O_3$@Zn, respectively.

Synthesis of δ-MnO_2 3D micro/nano spheres: δ-MnO_2 was synthesized by a hydrothermal method.[43] In brief, 6 mmol $KMnO_4$ and 1 mmol $MnSO_4 \cdot H_2O$ were dissolved in 70 mL distilled water under stirring. The precursor solution was transferred into a Teflon contained autoclave with a volume of 100 mL, and then heated at 180 °C for 12 h. After cooling to room temperature, the black precipitate was vacuum filtered until the PH reached to 7, and then dried at 100 °C in the air overnight.

2.2 Structural characterizations

The crystal structure of the Zn foils with and without Al_2O_3 coatings was confirmed by Powder X-ray diffraction (XRD, Bruker D8-Advance X-ray diffractometer) using Cu Kα radiation (1.54056 Å). The morphology was observed by using scanning electron microscope (SEM, Tescan MIRA3 FEG-ESEM) equipped with energy-dispersive X-ray spectroscopy (EDX). The microstructure of the Zn dendrites was examined by using high-resolution transmission electron microscope (HRTEM, FEI F30). The surface chemistry state was characterized by X-ray photoelectron spectroscopy (XPS, Axis Ultra DLD). The contact angle between Zn and the electrolyte was measured by a contact angle goniometer (Ramé Hart 260).

2.3 Electrochemical measurements

δ-MnO_2 (active material) was mixed with carbon black (Super P) and polyvinyldifluoride (PVDF) with a weight ratio of 7:2:1 in NMP solvent. The slurry was cast on a thin titanium foil (100 μm in thickness) by a doctor blade, and then dried under vacuum at 60 °C overnight. After that, the electrode was cut into round disks (Φ = 12 mm) for the cathode electrode in Zn-MnO_2 full cells. The mass loading

View Article Online
DOI: 10.1039/D0TA00748J

of MnO_2 was around 2.2 mg on each disk. CR2032 coin cells were assembled in the air atmosphere to evaluate the electrochemical performance of Zn−Zn symmetric cells, Zn−MnO_2 full cells. Zn−Zn symmetric cells were assembled with the same two zinc plates (Bare Zn or Al_2O_3 coated Zn), glass fibers (separator, Φ = 5/8 inch) and 3M $Zn(SO_3CF_3)_2$ aqueous electrolyte. Zn|MnO_2 full cells were constructed with δ-MnO_2 electrode as the cathode, bare Zn or 100Al_2O_3@Zn as the anode, a solution of 3M $Zn(SO_3CF_3)_2$ and 0.1 M $Mn(SO_3CF_3)_2$ as the electrolyte, and glass fibers (Φ = 5/8 inch) as the separator. All the galvanostatic charge/discharge was carried out in the voltage range of 0.8–1.8 V (vs. Zn^{2+}/Zn) on a Neware BTS 4000 battery tester. Cyclic voltammetry (CV), Electrochemical Impedance Spectroscopy (EIS) and liner polarization (corrosion test) was performed on a Biologic VSP Potentiostat/Galvanostat Station. CV was tested in the voltage range of 0.8–1.8 V (vs. Zn^{2+}/Zn) at a scan rate of 0.1 mV s^{-1}. EIS was conducted in a frequency range of 200 KHz to 10 mHz with a voltage amplitude of 5 mV. For corrosion test, the working (WE), counter (CE), and reference (REF) electrodes were zinc, platinum, and Ag/AgCl, respectively. Linear polarization technique was applied to the system by scanning between −0.7 and 0.4 V vs. Ag/AgCl from its open circuit voltage (OCV) at the rate of 3 mV s^{-1} in 3M $Zn(SO_3CF_3)_2$ solution. The surface area of the working electrode was 1.5 (1 × 1.5) cm^2, which was used to convert corrosion current (I_{corr}) to corrosion current density (j_{corr}). All the electrochemical testing was conducted at room temperature of 25°C. The charge and discharge specific capacities were calculated based on the MnO_2 loading weight in each cathode electrode.

3. Results and Discussion

View Article Online
DOI: 10.1039/D0TA00748J

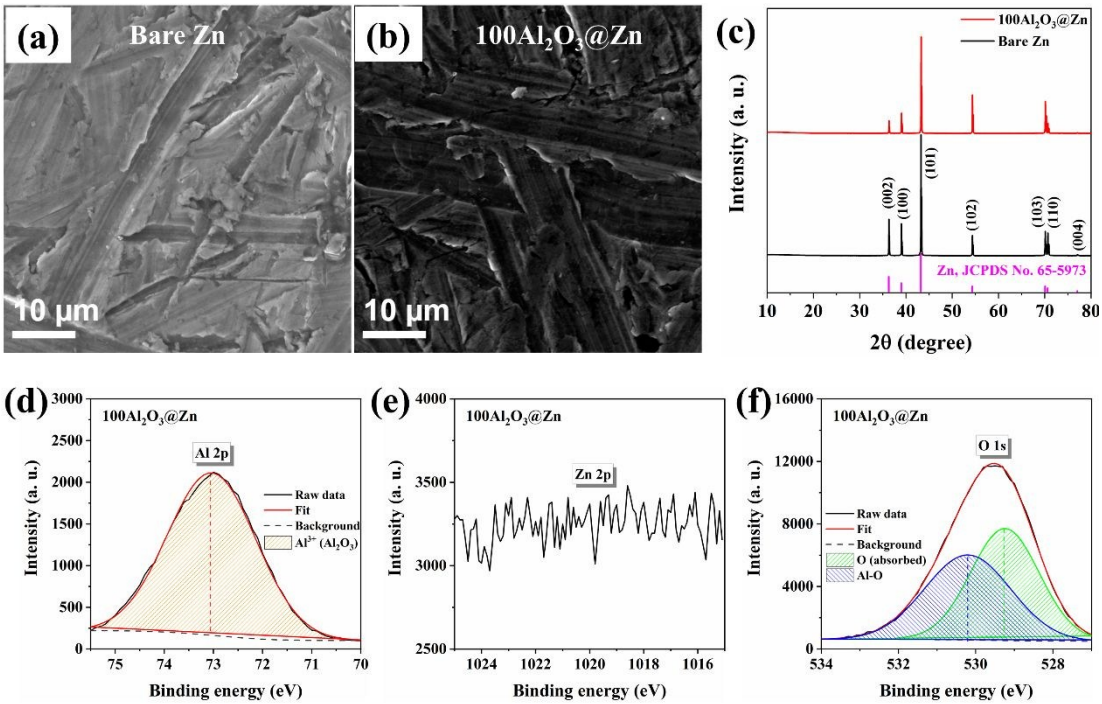

Figure 1. SEM images of bare Zn (a) and $100Al_2O_3$@Zn (b); XRD patterns of bare Zn and $100Al_2O_3$@Zn (c); High-resolution XPS spectra of Al 2p (d), Zn 2p (e) and O 1s (f) for $100Al_2O_3$@Zn.

Al_2O_3 coatings were performed on Zn foils by alternatively introducing TMA and H_2O using 30, 60, 100, and 200 cycles, corresponding to approximately 3, 6, 10, and 20 nm in the thickness based on the growth rate of ALD-Al_2O_3 (0.1nm per cycle).[39] The morphology, crystal structure, and surface chemistry of bare Zn and $100Al_2O_3$@Zn are characterized by SEM, XRD, and XPS, and the results are presented in **Figure 1**. As shown in **Figure 1a** and **1b**, bare Zn and $100Al_2O_3$@Zn possess a flat surface with microsized scratches resulting from the manufacturing process of Zn foils. Compared to bare Zn, $100Al_2O_3$@Zn looks much darker under SEM, mainly due to the insulating nature of Al_2O_3 coating. **Figure 1c** compares the XRD patterns of bare Zn and $100Al_2O_3$@Zn. As can be seen, the XRD pattern of bare Zn can be indexed as hexagonal Zn with P63/mmc space group (JCPDS No. 65-5973). $100Al_2O_3$@Zn shows the same XRD pattern as bare Zn, with no additional diffraction peaks of Al_2O_3, which is mainly due to the thin and amorphous nature of the ALD Al_2O_3 coating. Successful coating of Al_2O_3 on Zn foils is confirmed by EDX (**Figure S1a**) and XPS survey (**Figure S2)** analysis. For $100Al_2O_3$@Zn, the absence of Zn-related peaks (Zn 2p, Zn LMM, Zn 3p and Zn 3d) and the appearance of Al-related peaks (Al 2s and Al 2p) in the survey spectrum (**Figure S2c**) prove the successful deposition and uniform coverage

View Article Online
DOI: 10.1039/D0TA00748J

of Al_2O_3 on the surface of Zn plate by ALD. The chemical state of ALD Al_2O_3 coating is further analyzed by fitting the high-resolution spectra of Al 2p and O 1s and the results are shown in **Figure 1d-1f**. In **Figure 1d**, a symmetric peak of Al 2p at 72.9 eV is assigned to Al_2O_3 on the surface of $100Al_2O_3$@Zn.[38,43] As shown in **Figure 1f**, the O1s spectrum of $100Al_2O_3$@Zn is not symmetric and can be fitted into two peaks at 529.3 eV and 530.2 eV, which are attributed to absorbed oxygen and Al-O bond in Al_2O_3, respectively.[44,45] The absorbed oxygen species may come from the environment due to the adsorption capability of ALD Al_2O_3 film with oxygen in the air before transferring into XPS chamber. Additionally, the C 1s core levels of $100Al_2O_3$@Zn (**Figure S3**) can be fitted into two peaks at 284.6 eV (C-C) and 286 eV (C-O-C), which may be attributed to adventitious carbon. Based on the above results, it can be concluded that Al_2O_3 coating layer was successfully deposited on the surface of Zn foils by ALD.

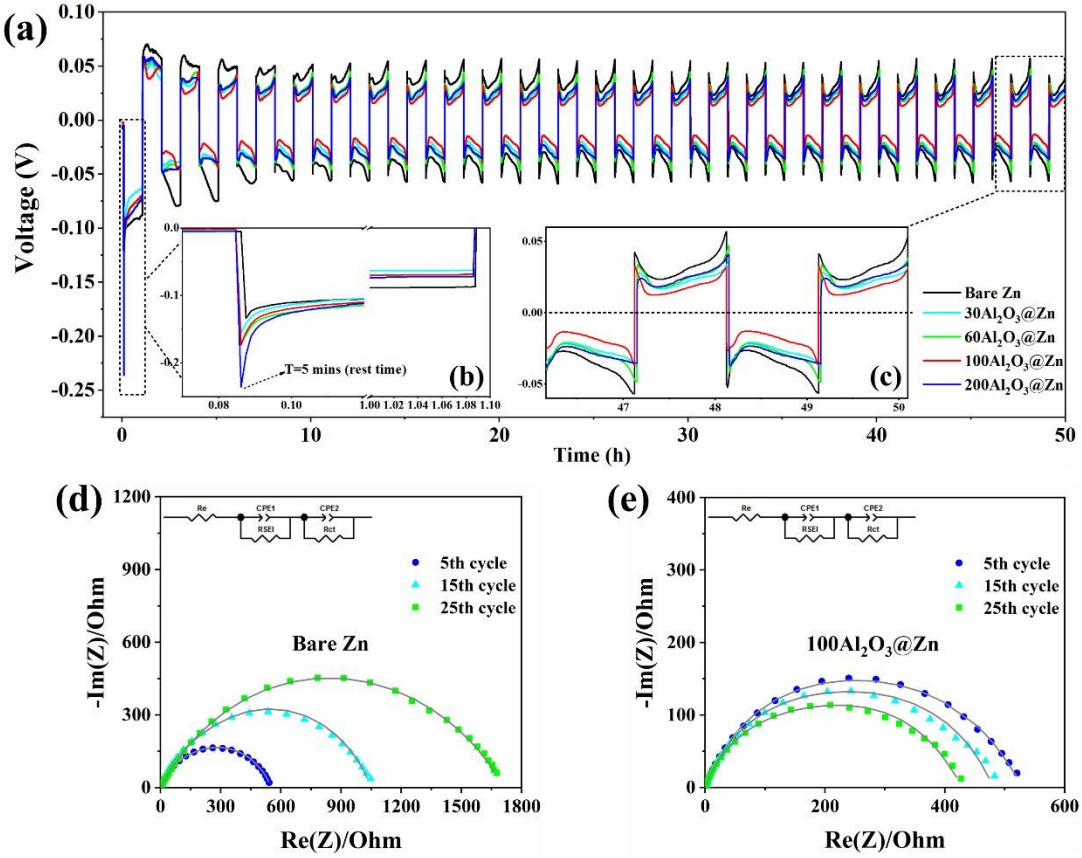

Figure 2. (a, b, c) Charge-discharge profiles for Zn|Zn symmetric cells with bare Zn, $30Al_2O_3$@Zn, $60Al_2O_3$@Zn, $100Al_2O_3$@Zn, and $200Al_2O_3$@Zn. The EIS of Zn|Zn symmetric cells with bare Zn (d) and $100Al_2O_3$@Zn (e) anodes at the

View Article Online
DOI: 10.1039/D0TA00748J

end of charge process in the 5th (10 h), 15th (30 h) and 25th (50 h) cycle.

The effect of Al_2O_3 coating thickness on the Zn stripping/plating behavior was first investigated in Zn|Zn symmetric cells, and the results are presented in **Figure 2**. For fair comparison, 200 μL of 3M $Zn(SO_3CF_3)_2$ aqueous electrolyte was added into each cell, and the current density and areal capacity was set as 1 mA cm^{-2} and 1 mAh cm^{-2}, respectively. As seen in the charge/discharge profiles (**Figure 2a, 2b,** and **2c**), zinc nucleation overpotential (ZNO) is required to initiate Zn plating and stripping process for all the samples. ZNO is related to not only Zn^{2+} and e^- transfer resistance, but also the kinetics of Zn stripping/plating reactions. In general, the Zn^{2+} and e^- transfer resistance is regarded as intrinsic property of the electrolyte and electrode employed.[24,46] However, kinetics of Zn stripping/plating reactions depends on several factors, such as Zn nuclei size and size distribution, surface tension and morphology of nucleation substrates. As displayed in **Figure 2b**, in the first discharge process, ZNO value of Zn|Zn cells gradually increases with elevating ALD cycle numbers from 0 to 200. The ZNO value is determined as -133.9, -155.6, -169.5, -173.3 and -235.9 mV, for bare Zn, $30Al_2O_3$@Zn, $60Al_2O_3$@Zn, $100Al_2O_3$@Zn, and $200Al_2O_3$@Zn, respectively. This result indicates that higher initial overpotential is required for Zn plates with Al_2O_3 coatings to start the Zn plating/stripping process, possibly due to the insulating nature of ALD Al_2O_3 coating layers on the Zn electrode. Despite of the higher ZNOs at beginning of the first discharge process, Al_2O_3 coated Zn anodes show quickly reduced overpotentials as the first discharge cycle goes on (Figure2a, at T=1.083 h). This phenomenon suggests an activation process of Al_2O_3 coating on the Zn anode during the first cycle. Furthermore, as shown in **Figure 2c**, $100Al_2O_3$@Zn exhibits the lowest overall voltage hysteresis (T=46−50 h) among all the samples, indicating its fastest kinetics of Zn^{2+} in the stripping and plating process. To get better understanding on the ALD Al_2O_3 coating effect, electrochemical impedance spectroscopy (EIS) of bare Zn and $100Al_2O_3$@Zn symmetric cells was performed at the three different time during cycling (5^{th}, 15^{th}, 25^{th} cycle). As shown in **Figure 2d** and **2e**, all the EIS plots featured with depressed semicircle, which can not be fitted into one single semicircle. By fitting the EIS with the equivalent circuit (inset in **Figure 2d** and **2e**), the fitting curve matched well with the raw data, indicating the suitability of the employed equivalent circuit. The calculated impendence parameters (R_e, R_{SEI} and R_{ct}) were shown in **Table 1**. The continuous growth of the R_{SEI} and R_{ct} of bare Zn suggest a deteriorated electrode/electrolyte interface

View Article Online
DOI: 10.1039/D0TA00748J

during the Zn stripping/plating cycling process. In contrast, for $100Al_2O_3$@Zn, it shows a decreased R_{ct} value, indicating suppressed side reaction at the electrode/electrolyte interface. The trend in the EIS data demonstrated that the ALD Al_2O_3 coating can reduce the reactivity between the Zn electrode and the electrolyte upon cycling, thus leading to lower impendences and overpotential and enhanced the Zn plating/stripping kinetics reaction.[37,38]

	Bare Zn			**$100Al_2O_3$@Zn**		
	5th	15th	25th	5th	15th	25th
R_e /Ω	1.0	1.0	5.3	0.8	1.0	1.9
R_{SEI} /Ω	39.5	74.2	400.7	150.2	164.0	179.2
R_{ct} /Ω	512.8	974.5	1311.0	375.6	314.4	224.1

Table 1. The impedance parameters for bare Zn and $100Al_2O_3$@Zn in the 5th, 15th and 25th cycle.

The amount of electrolytes is a critical factor for the energy density of metal anode batteries, and has been rarely investigated in ZIBs.[36] Excessive amount of electrolyte always improves the results from half-cell tests and meanwhile could lower the energy density of batteries, although it is not the case in practical application and becomes defaulted in the lab test. The Al_2O_3 coating effect on Zn striping and plating process was studied in Zn|Zn symmetric cells using different amounts (200 μL, 50 μL, and 25 μL) of 3M $Zn(SO_3CF_3)_2$ aqueous electrolyte. The optimized $100Al_2O_3$@Zn and bare Zn are employed for comparison, and the results are shown in **Figure 3a-f**. As can be seen, 50 μL and 25 μL, the lifespan of bare Zn shortens from over 100 hours to only about 70 hours, before internal short circuit occurs. In contrast, $100Al_2O_3$@Zn maintains a good stability over 100 hours, regardless of the electrolyte amounts studied. Moreover, close examination on the voltage vs. time profiles in the 35th cycle (**Figure 3d, 3e,** and **3f**) discloses a lower voltage hysteresis for $100Al_2O_3$@Zn than bare Zn. These results strongly suggest that the amount of electrolyte has significant influence on the lifetime of Zn|Zn symmetric cells. Although the flooded electrolyte could improve the lifespan of bare Zn anode, it will reduce energy density at the cell level because of the extra weight added. While for the Zn anode with Al_2O_3 coating, it

View Article Online
DOI: 10.1039/D0TA00748J

still exhibited comparable cycling performance even with less amount of electrolyte. This advantage will become more obvious when taking consideration of raw materials cost and battery energy density in practical production. Because of the better surface wettability by ALD Al_2O_3 coating, it will make the utmost of electrolyte during the repeated Zn stripping/plating cycles, thus leading to good electrochemical performance even using less electrolyte. Furthermore, the charging-discharging ability of bare Zn and $100Al_2O_3$@Zn at high current densities of 2 mA cm^{-2} and 3 mA cm^{-2} were shown in **Fig. S5**. As displayed, $100Al_2O_3$@Zn exhibited better cycling stability and lower overpotential than bare Zn at high current densities. Specifically, the lifespan of bare Zn was shortened to 20 h and 12 h, at a current density of 2 and 3 mA cm^{-2} respectively. In contrast, $100Al_2O_3$@Zn showed better cycling stability without voltage fluctuations during the stripping/plating process. This result demonstrates that the Al_2O_3 ALD coating can improve the cycling life of Zn anode even at high current densities. The above results demonstrate that Al_2O_3 coating by ALD not only improves the cycling life of Zn anode, but also reduce voltage hysteresis during Zn stripping and plating process, whether cycling within less electrolyte or at higher current densities.

Long-term cycling stability of $100Al_2O_3$@Zn and bare Zn was further tested in a Zn|Zn symmetric cell configuration, and the results are shown in **Figure 3g**. Compared with bare Zn, the $100Al_2O_3$@Zn exhibits significantly enhanced lifetime and small voltage hysteresis during repeated Zn plating and stripping process. For example, the bare Zn shows a voltage hysteresis as high as 73.5 mV, and its voltage profiles becomes fluctuated after 242 h, probably due to internal short circuit resulting from Zn dendrites. In comparison, the voltage profiles of $100Al_2O_3$@Zn keep very stable for over 500 h without any voltage fluctuation and short circuit. In addition, $100Al_2O_3$@Zn exhibits a voltage hysteresis of 36.5 mV, much lower than that of bare Zn (73.5 mV), during Zn stripping and plating process. Furthermore, the voltage vs. capacity profiles of bare Zn and $100Al_2O_3$@Zn for the selected cycles are displayed in **Figure 3h**. For $100Al_2O_3$@Zn, a flat voltage plateau at both the charge and discharge states can be retained without obvious increases in voltage hysteresis throughout the whole cycling process. The capacity profiles of $100Al_2O_3$@Zn are nearly overlapped, indicating a very stable cycling ability stemming from the ALD Al_2O_3 coating. For bare Zn, however, the voltage profiles become more separated with cycling, suggesting unstable Zn stripping and plating behavior on the bare Zn anode. The long-term cycling

View Article Online
DOI: 10.1039/D0TA00748J

performance highly demonstrate that ALD Al_2O_3 coating can not only improve the lifespan, especially with small electrolyte amount, but also reduce the voltage overpotential and hysteresis of Zn symmetric cells during repeating Zn stripping/plating cycles.

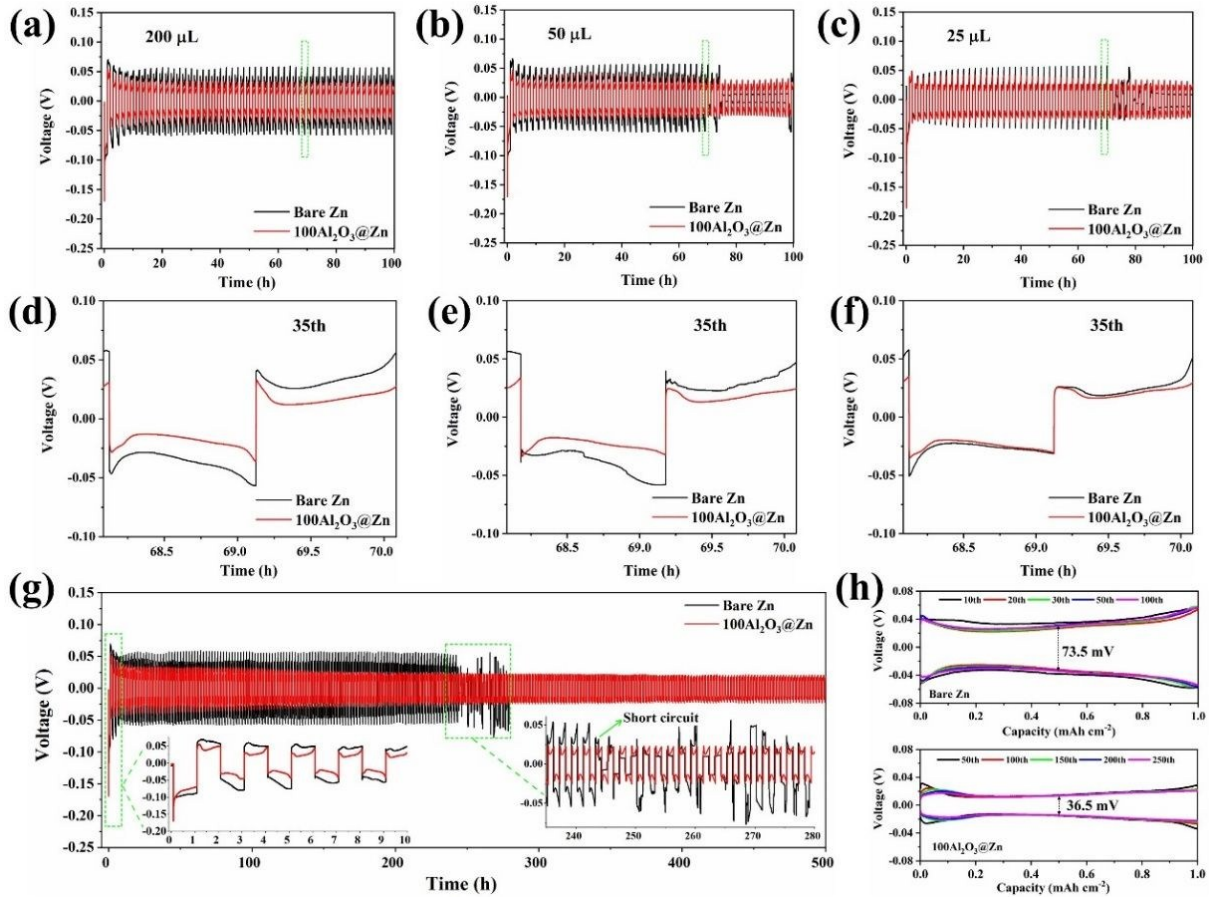

Figure 3. Charge-discharge profiles of bare Zn and $100Al_2O_3$@Zn symmetric cells with different amounts of electrolyte: (a, d) 200 µL, (b, e) 50 µL and (c, f) 25 µL; (g) long-term cycling stability of the bare Zn and $100Al_2O_3$@Zn with 200-µL electrolyte; (h) voltage vs. capacity profiles of bare Zn and $100Al_2O_3$@Zn in 10^{th}, 20^{th}, 30^{th}, 50^{th} and 100^{th} cycles. All the cells are cycled at a current density of 1 mA cm^{-2} with an areal capacity of 1 mAh cm^{-2}.

In order to understand the reasons for the improved performance by Al_2O_3 coating, SEM was used to examine the top-view and cross-sectional morphologies of Zn anode with/without Al_2O_3 coating after cycling and the glass-fiber separators recovered from the cycled Zn|Zn cells. As shown in **Figure 4a-d**, the cycled bare Zn possesses a severely corroded rough surface covered with vertically aligned thin and

View Article Online
DOI: 10.1039/D0TA00748J

sharp Zn dendrite flakes. In contrast, $100Al_2O_3$@Zn presents a clean and flat surface with much less Zn dendrite flakes (**Figure 4c-f**). As expected, the Zn anodes with other different ALD cycle numbers (**Figure S6**) also present smoother surface than the bared one. The SEM results strongly proves that ALD Al_2O_3 coating effectively inhibited the growth of Zn dendrites on the Zn anode, resulting in a smoother Zn surface and thus improving the cycling of batteries. Furthermore, the glass-fiber separators from the cycled bare Zn an $100Al_2O_3$@Zn symmetric cells were also observed by SEM (**Figure S7**). As can be seen from **Figure S7a** and the insert, the separator from the bare Zn cell has accumulated a large amount of Zn deposition, which is further confirmed by the strong Zn peak in the EDX spectrum (**Figure S7c**). The glass-fiber separator is largely blocked with many Zn dendrites, which might hinder zinc ion diffusion through the separator, lead to the loss of active Zn metal, and cause internal short circuit. Collectively, these factors could result in an increased cell resistance, low Zn stripping and plating efficiency, and deteriorated electrochemical performance. In sharp contrast, the separator from $100Al_2O_3$@Zn (**Figure 7b** and insert) has a much cleaner surface than that of bare Zn, with little Zn deposition. From Figure4, it is evident that by ALD Al_2O_3 coating effectively inhibited the growth of Zn dendrites on the Zn anode, and reduced the trapping of Zn in the separator, leading to improved electrochemical performance in Zn|Zn cells.

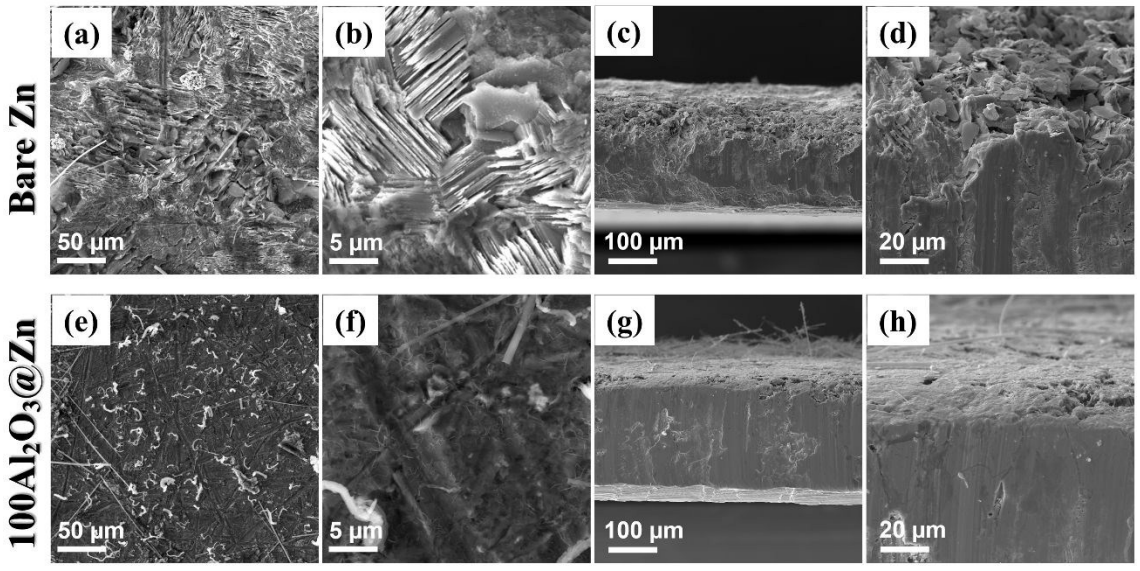

Figure 4. Top-view (a, b) and cross-sectional (c, d) morphologies of cycled bare Zn; Top-view (e, f) and cross-sectional

View Article Online
DOI: 10.1039/D0TA00748J

(g, h) morphologies of cycled $100Al_2O_3$@Zn

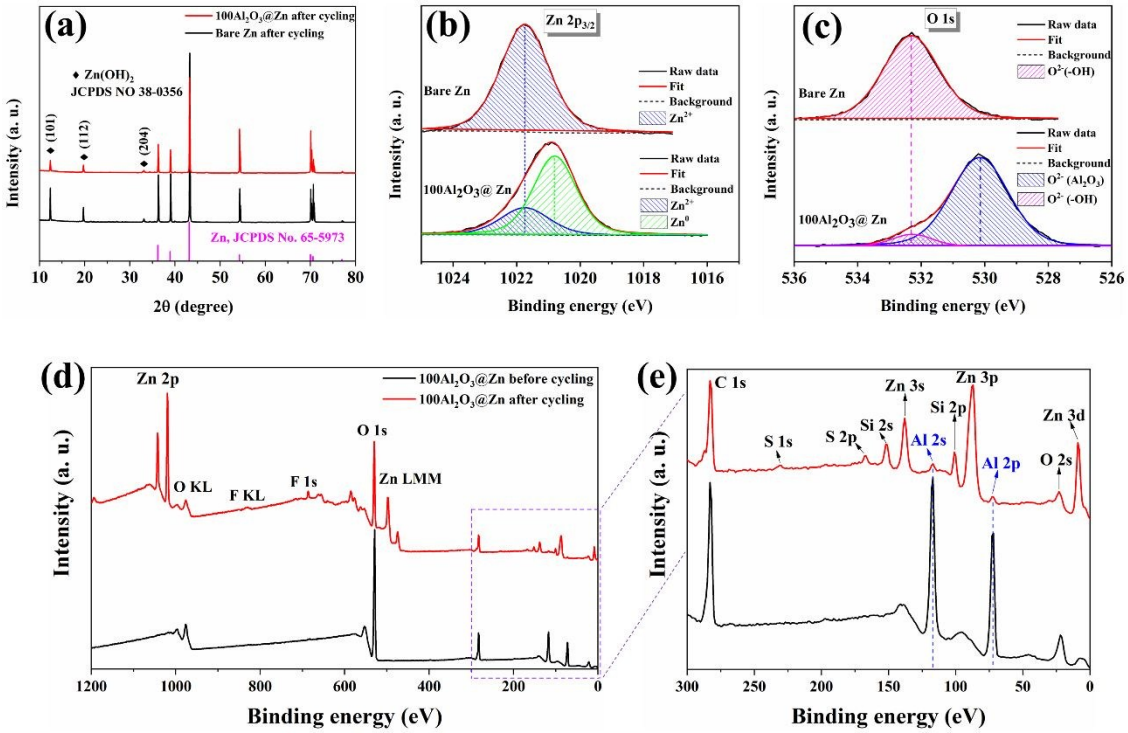

Figure 5. (a) XRD patterns of bare Zn and $100Al_2O_3$@Zn after cycling; XPS spectra of (b) Zn 2p and (dc) O 1s for bare Zn and $100Al_2O_3$@Zn after cycling. (d) XPS survey spectra of $100Al_2O_3$@Zn before and after cycling. (e) the enlarged area from 300 ~ 0 eV

In order to get deep understanding on the structure and composition of Zn dendrites, XRD and XPS were utilized to characterize the bare Zn and $100Al_2O_3$@Zn recycled from Zn|Zn symmetric cells. As shown in **Figure 5a**, for besides the diffraction peaks assignable to Zn metal (JCPDS No. 65-5973), three new diffraction peaks are identified at 12.4°, 19.6° and 33.1°, respectively, for both cycled bare Zn and $100Al_2O_3$@Zn, and are characteristic peaks of $Zn(OH)_2$ (JCPDS No. 65-5973).[47] This suggests that the Zn dendrite flakes in **Figure 4** are composed of $Zn(OH)_2$ species. This conclusion was also consistent with the HETEM results of cycles bare Zn (**Figure S8**). In addition, the peak intensities of $Zn(OH)_2$ are much weaker in cycled $100Al_2O_3$@Zn than bare Zn, revealing the suppressed formation of $Zn(OH)_2$ by Al_2O_3 coating. XPS was employed to determine the chemical state on the Zn anode surface after cycling.

View Article Online
DOI: 10.1039/D0TA00748J

Prior to XPS measurements, the Zn anode were thoroughly washed with deionized water to remove residual salt and glass fiber. In order to reveal the chemical species of Zn dendrites on the surface of zinc anode, high-resolution Zn 2p and O1s spectra were recorded and displayed in **Figure 5b** and **5c**, respectively. For $100Al_2O_3$@Zn after cycling, the Zn 2p peak is asymmetric in the shape with a visible shoulder on the low energy side, indicating at least two different bonds. A Gauss-Lorentz fit yields a main peak at 1020.8 eV and a shoulder peak at 1021.7 eV, which is assigned to Zn metal and $Zn(OH)_2$, respectively.[48, 49] On the contrary, the Zn 2p spectrum of cycled bare Zn shows a symmetric peak being fitted into one peak at 1021.7 eV, which is characteristic of $Zn(OH)_2$. The analysis on Zn2p spectra of cycled bare Zn and $100Al_2O_3$@Zn confirms that the formation of $Zn(OH)_2$ is largely suppressed due to ALD Al_2O_3 coating. As shown in **Figure 5c**, the asymmetric O 1s spectrum of cycled $100Al_2O_3$@Zn is composed of a major peak at 530.2 eV (O^{2-} in Al_2O_3) and a minor peak at 532.3 eV assignable to hydroxide (OH^-).[50] While for the cycled bare Zn, the symmetric O 1s spectrum is fitted well into only one peak at 532.3 eV, which is ascribed to the hydroxide. Based on the Zn 2p and O 1s XPS results, it can be found that the Zn dendrites contain $Zn(OH)_2$, which is non-conductive and might create an insulating barrier for Zn ion diffusion. With the surface modification of Al_2O_3 coating on Zn anode, $Zn(OH)_2$ can be effectively reduced, consequently leading to improved Zn stripping/plating reversibility. For a better comparison, we compare the full survey XPS spectra of $100Al_2O_3$@Zn before and after cycling and local region in the Al 2s and Al 2p peaks (300-0 eV). As shown in **Figure 5d**, for $100Al_2O_3$@Zn before cycling, there is no Zn-related XPS peaks (Zn 2p, Zn LMM, etc.) and obvious Al-related peaks (Al 2s and Al 2p), indicating the successful coating of Al_2O_3 on the surface of Zn anode. In **Figure 5e**, it is clear that Al XPS peaks located at about 117.3 eV (Al 2s) and 72.3 eV (Al 2p) can still be observed, but their intensities decreased to a significantly lower value. This is expected and consistent with the reported ALD Al_2O_3 coating on Li metal.[38] Although the Al content detected by XPS decreased to a very low value on the Zn surface after prolonged Zn striping/plating cycles, the improved morphology without large Zn dendrite flakes could be observed after extended cycling. This suggests that the significant impact of ALD Al_2O_3 on suppressing dendrite formation and improving the cycling performance even after Al_2O_3 film undergoes some mechanical degradation.

View Article Online
DOI: 10.1039/D0TA00748J

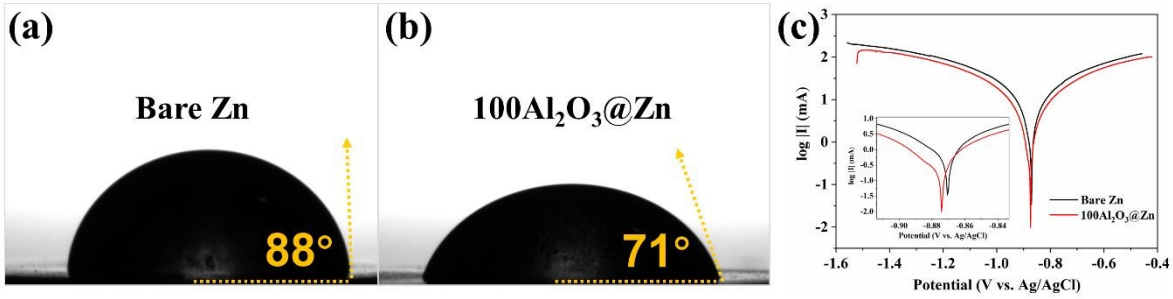

Figure 6. Contact angles of (a) bare Zn and (b)$100Al_2O_3$@Zn with 3M $Zn(SO_3CF_3)_2$ electrolyte; (c) corrosion curves of bare Zn and $100Al_2O_3$@Zn in 3M $Zn(SO_3CF_3)_2$ electrolyte.

The influence of ALD Al_2O_3 coating on the zinc surface were also investigated by contact angle measurement and corrosion test in a 3M $Zn(SO_3CF_3)_2$ aqueous solution. For the contact angle measurement, the electrolyte droplet was kept as 5 μL to avoid gravitational effect. As shown in **Figure 6a** and **6b**, $100Al_2O_3$@Zn has a contact angle of 71°, lower than than that of bare Zn (88°), indicating a better surface wettability between the zinc plate and electrolyte caused by ALD Al_2O_3 coating. The improved surface wettability could result in a more even Zn ion flux across the Zn surface and lower charge transfer resistance during Zn stripping and plating process, which are beneficial for the electrochemical performance.[30,36] The corrosion curves of Zn with and without Al_2O_3 coating were shown in **Figure 6c**, and the corresponding Tafel fit corrosion kinetic parameters were summarized in **Table S2**. As shown in **Figure 6c** and the insert, the corrosion potential of Zn foil with Al_2O_3 coating shifts to more negative potential and the corrosion current becomes smaller. For example, the corrosion potential of bare Zn and $100Al_2O_3$@Zn is -871.1 mV and -875.7 mV (vs. Ag/AgCl), respectively, indicating improved corrosion resistance by Al_2O_3 coating. This conclusion is further confirmed by the lower corrosion current of $100Al_2O_3$@Zn (4.91 mA) than that of bare Zn (8.20 mA). The corrosion test results indicate that Al_2O_3 coating layer can act as inhibitor to alleviate Zn metal from corrosion reaction.

The Zn anodes with and without ALD coating were further applied in Zn-MnO_2 cells using δ-MnO_2 3D micro/nano spheres as cathode (**Figure S9**) for full-cell validation. Cycling voltammetry (CV) was first used to investigate the redox reactions and the reversibility of bare Zn-MnO_2 and $100Al_2O_3$@Zn-MnO_2 cells for the initial three cycles during the charge-discharge process. As shown in **Figure S10**, after

View Article Online
DOI: 10.1039/D0TA00748J

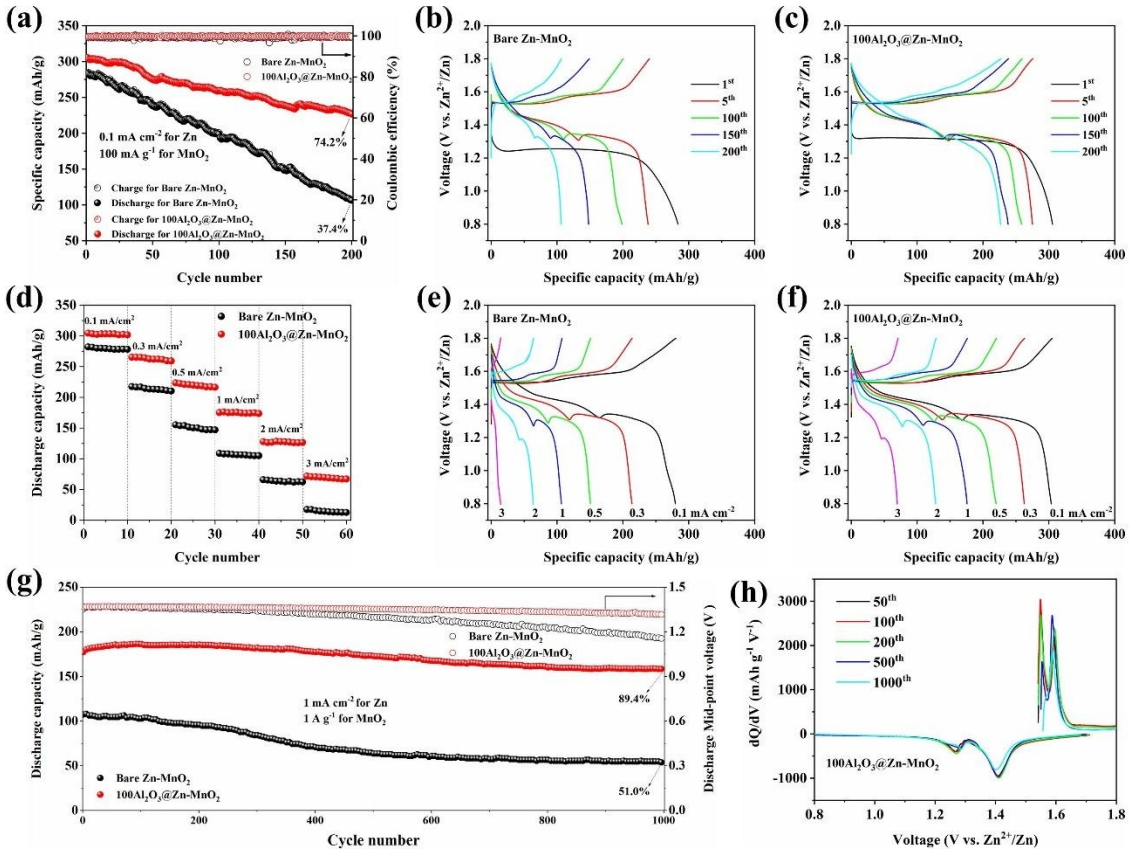

Figure 7. (a) Cycling performance of $100Al_2O_3$@Zn-MnO_2 cell and bare Zn-MnO_2 cell at 0.1 mA cm^{-2} (corresponding to 100 mA g^{-1} (1/3 C) for MnO_2); charge-discharge profiles of (b) bare Zn-MnO_2 cell and (c) $100Al_2O_3$@Zn-MnO_2 cell in the 1st, 5th, 100th, 150th and 200th cycle; (d) Rate capability of $100Al_2O_3$@Zn-MnO_2 cell and bare Zn-MnO_2 cell ranging from 0.1 to 3 mA cm^{-2}; charge-discharge profiles of (e) bare Zn-MnO_2 cell and (f) $100Al_2O_3$@Zn-MnO_2 cell ranging from 0.1 to 3 mA cm^{-2}; (g) long-term cycling stability and discharge mid-point voltage of $100Al_2O_3$@Zn-MnO_2 cell and bare Zn-MnO_2 cell at 1 mA cm^{-2} (corresponding to 1 A g^{-1} (3.33 C) for MnO_2), and (h) differential capacity (dQ/dV) plots of $100Al_2O_3$@Zn-MnO_2 cell in the 50th, 100th, 200th, 500th and 100th cycles.

the reduction reaction peak (at 1.10V) in the first cycle, the CV curve of bare Zn-MnO_2 has two pairs of reduction/oxidation peaks located at 1.14/1.37 and 1.57/1.61 V, while $100Al_2O_3$@Zn-MnO_2 has also two pairs at 1.15/1.38 and 1.56/1.60 V, indicating a similar redox reaction behavior. Therefore, ALD Al_2O_3 coating does not change the mechanism of redox reactions in δ-MnO_2 cathode. **Figure 7a** shows the cycling performance of bare Zn-MnO_2 and $100Al_2O_3$@Zn-MnO_2 at 0.1 mA cm^{-2} (corresponding to 100 mA g^{-1} (1/3 C) for MnO_2 cathode) for 200 cycles. $100Al_2O_3$@Zn-MnO_2 displays much better cycling-

View Article Online
DOI: 10.1039/D0TA00748J

stability than the bare Zn-MnO_2. The discharge capacity of bare Zn-MnO_2 decreases from 283.8 mAh g^{-1} in the 1st cycle to 106.2 mAh g^{-1} in the 200th cycle, with a capacity retention of 37.4% after 200 cycles. In contrast, 100Al_2O_3@Zn-MnO_2 exhibits a discharge capacity of 305.5 mAh g^{-1} in the 1st cycle, and maintains a discharge capacity of 226.7 mAh g^{-1} after 200 cycles, with a high capacity retention of 74.2%. Moreover, the CE of 100Al_2O_3@Zn-MnO_2 is also much improved compared to bare Zn-MnO_2. The charge-discharge profiles in the 1st, 5th, 100th, 150th, and 200th cycles of bare Zn-MnO_2 cell and 100Al_2O_3@Zn-MnO_2 cell are shown in **Figure 7b** and **7c**, respectively. After the first discharge cycle, the following discharge curves are divided into two obvious platforms with a turning point at 1.30 V. As previously reported in aqueous Zn-MnO_2 batteries,[12,36,52] the first discharge plateau before 1.30 V is dominated by the insertion of H^+, and the second one after 1.30 V corresponds to the Zn^{2+} insertion into MnO_2. 100Al_2O_3@Zn-MnO_2 has much smaller polarization than bare Zn-MnO_2. The voltage plateaus during charge and discharge process agree well with the CV results. These results suggest that ALD Al_2O_3 coating can enhance the cycling stability and reduce the electrode polarization during the charge-discharge process. The rate capabilities of bare Zn-MnO_2 and 100Al_2O_3@Zn-MnO_2 battery are displayed in **Figure 7d** and the corresponding charge–discharge curves at each current density are shown in **Figure 7e** and **7f**. As clearly seen from **Figure 7d**, 100Al_2O_3@Zn-MnO_2 shows a more superior rate capability than bare Zn-MnO_2 at all the current densities. For example, 100Al_2O_3@Zn-MnO_2 delivers a reversible capacity of average 303 mA h g^{-1}, about 98.4% of its theoretical capacity (308 mAh g^{-1}), at 0.1 mA cm^{-2} (100 mA g^{-1} for MnO_2). When the current increases from 0.1 to 0.3, 0.5, 1 and 2 mA cm^{-2} (300, 500, 1000 and 2000 mA g^{-1} for MnO_2), the discharge capacity can reach 262.7, 219.6, 174.9 and 127.2 mAh g^{-1}, respectively. It still can deliver a discharge capacity of 69.2 mAh g^{-1}, even at a current as high as 3 mA cm^{-2} (3 A g^{-1} or ≈ 10 C for MnO_2). In contrast, for bare Zn-MnO_2, its discharge capacities are about 279.6, 213.9, 150.6, 106.7 and 63.7 mAh g^{-1} ranging from 0.1 to 2 mA cm^{-2}, and only delivers ~ 15 mAh g^{-1} at a current of 3 mA cm^{-2}. Furthermore, the characteristic turning point and plateaus can still be easily distinguished in charge-discharge curves of 100Al_2O_3@Zn-MnO_2 (**Figure 7f**), even at the high current density of 3 mA cm^{-2}, while it is not the case for bare Zn-MnO_2 (**Figure 7e**). The long-term cycling stability is further evaluated at 1 mA cm^{-2} (1 A g^{-1} for MnO_2). As shown in **Figure 7g**, for 100Al_2O_3@Zn-MnO_2, a discharge capacity of 158.4 mAh g^{-1} is retained even after 1000 cycles, with a high capacity

View Article Online
DOI: 10.1039/D0TA00748J

retention of 89.4%. 100Al_2O_3@Zn-MnO_2 exhibits overlapped charge-discharge profiles in the 50th, 100th, 200th, 500th, and 1000th cycles (**Figure S11**) and dQ/dV plots (**Figure 7h**), demonstrating a high cycling stability and reversibility. On the contrary, the capacity of bare Zn-MnO_2 shows a suddent decrease after 400 cycles and finally stabilizes at 54.7 mAh g^{-1} after 1000 cycles with a capacity retention of only 51.0%. In addition, the discharge mid-point voltage of 100Al_2O_3@Zn-MnO_2 (1.32 V in the 1000th cycle) exhibits a much higher stability than that of bare Zn-MnO_2 (1.15 V in the 1000th cycle) during the whole cycling process, suggesting that ALD Al_2O_3 coating improves the capacity retention, reduce discharge voltage decay, and increase the energy density of ZIBs.

3. Conclusions

In conclusion, we have successfully demonstrated the ALD Al_2O_3 coating as a thin protective layer on the Zn metal for constructing robust Zn anode in aqueous ZIBs for the first time. The nanoscale ultrathin Al_2O_3 coating reduced the Zn anode reactivity with the electrolyte, improved the uniformity of Zn plating/stripping, and suppressed the formation of Zn dendrites, thus significantly improving the lifespan of Zn-Zn symmetric cells. Superior batteries performance was achieved when Zn metal with optimized Al_2O_3 coating (~ 10 nm) applied as an anode in Zn-MnO_2 batteries. The presented design of ALD Al_2O_3 coated metal Zn anode may bring in new opportunities to the realization of safe and eco-friendly aqueous ZIBs and shed light on the development of other metal anode-based battery systems.

Acknowledgements

This work was supported by Nature Sciences and Engineering Research Council of Canada (NSERC), Canada Foundation for Innovation (CFI), BC Knowledge Development Fund (BCKDF), and the University of British Columbia (UBC). Special thanks to 4D Labs at Simon Fraser University (SFU) for XPS characterization.

References

[1] M. Armand and J.-M. Tarascon, *Nature*, 2008, **451**, 652.

[2] B. Dunn, H. Kamath and J.-M. Tarascon, *Science*, 2011, **334**, 928-935.

View Article Online
DOI: 10.1039/D0TA00748J

[3] J. B. Goodenough and Y. Kim, *Chem. Mater.*, 2009, **22**, 587-603.

[4] N. Yabuuchi, K. Kubota, M. Dahbi and S. Komaba, *Chem. Rev.*, 2014, **114**, 11636-11682.

[5] J. C. Pramudita, D. Sehrawat, D. Goonetilleke and N. Sharma, *Adv. Energy Mater.*, 2017, **7**, 1602911.

[6] G. Fang, J. Zhou, A. Pan and S. Liang, *Acs Energy Lett*, 2018, **3**, 2480-2501.

[7] X. Zeng, J. Hao, Z. Wang, J. Mao and Z. Guo, *Energy Storage Mater*, 2019.

[8] H. Li, L. Ma, C. Han, Z. Wang, Z. Liu, Z. Tang and C. Zhi, *Nano Energy*, 2019.

[9] M. Song, H. Tan, D. Chao and H. J. Fan, *Adv. Funct. Mater.*, 2018, **28**, 1802564.

[10] M. Winter and R. J. Brodd, *Chem. Rev.*, 2005, **105**, 1021-1021.

[11] Y. Wang and W. H. Zhong, *Chemelectrochem*, 2015, **2**, 22-36.

[12] H. Pan, Y. Shao, P. Yan, Y. Cheng, K. S. Han, Z. Nie, C. Wang, J. Yang, X. Li and P. Bhattacharya, *Nature Energy*, 2016, **1**, 16039.

[13] N. Zhang, F. Cheng, Y. Liu, Q. Zhao, K. Lei, C. Chen, X. Liu and J. Chen, *J. Am. Chem. Soc.*, 2016, **138**, 12894-12901.

[14] H. Liang, Z. Cao, F. Ming, W. Zhang, D. H. Anjum, Y. Cui, L. Cavallo and H. N. Alshareef, *Nano Lett.*, 2019.

[15] F. Wang, O. Borodin, T. Gao, X. Fan, W. Sun, F. Han, A. Faraone, J. A. Dura, K. Xu and C. Wang, *Nature materials*, 2018, **17**, 543.

[16] D. Kundu, B. D. Adams, V. Duffort, S. H. Vajargah and L. F. Nazar, *Nature Energy*, 2016, **1**, 16119.

[17] T.-H. Wu, Y. Zhang, Z. D. Althouse and N. Liu, *Materials Today Nano*, 2019, 100032.

[18] S. Higashi, S. W. Lee, J. S. Lee, K. Takechi and Y. Cui, *Nat Commun*, 2016, **7**, 11801.

[19] Q. Yang, G. Liang, Y. Guo, Z. Liu, B. Yan, D. Wang, Z. Huang, X. Li, J. Fan and C. Zhi, *Adv. Mater.*, 2019, **31**, 1903778.

[20] X. G. Zhang, *J. Power Sources*, 2006, **163**, 591-597.

[21] J. F. Parker, C. N. Chervin, I. R. Pala, M. Machler, M. F. Burz, J. W. Long and D. R. Rolison, *Science*, 2017, **356**, 415-418.

View Article Online
DOI: 10.1039/D0TA00748J

[22] D. Chao, C. Zhu, M. Song, P. Liang, X. Zhang, N. H. Tiep, H. Zhao, J. Wang, R. Wang and H. Zhang, *Adv. Mater.*, 2018, **30**, 1803181.

[23] D. E. Turney, J. W. Gallaway, G. G. Yadav, R. Ramirez, M. Nyce, S. Banerjee, Y.-c. K. Chen-Wiegart, J. Wang, M. J. D'Ambrose and S. Kolhekar, *Chem. Mater.*, 2017, **29**, 4819-4832.

[24] M. Cui, Y. Xiao, L. Kang, W. Du, Y. Gao, X. Sun, Y. Zhou, X. Li, H. Li and F. Jiang, *ACS Appl Energ Mater*, 2019, **2**, 6490-6496.

[25] D. Stock, S. Dongmo, K. Miyazaki, T. Abe, J. Janek and D. Schröder, *J. Power Sources*, 2018, **395**, 195-204.

[26] Z. Zhao, J. Zhao, Z. Hu, J. Li, J. Li, Y. Zhang, C. Wang and G. Cui, *Energy Environ. Sci.*, 2019.

[27] W. Li, K. Wang, M. Zhou, H. Zhan, S. Cheng and K. Jiang, *Acs Appl Mater Inter*, 2018, **10**, 22059-22066.

[28] A. Xia, X. Pu, Y. Tao, H. Liu and Y. Wang, *Appl. Surf. Sci.*, 2019, **481**, 852-859.

[29] Z. Zhou, Y. Zhang, P. Chen, Y. Wu, H. Yang, H. Ding, Y. Zhang, Z. Wang, X. Du and N. Liu, *Chem. Eng. Sci.*, 2019, **194**, 142-147.

[30] L. Kang, M. Cui, F. Jiang, Y. Gao, H. Luo, J. Liu, W. Liang and C. Zhi, *Adv. Energy Mater.*, 2018, **8**, 1801090.

[31] W. Dong, J.-L. Shi, T.-S. Wang, Y.-X. Yin, C.-R. Wang and Y.-G. Guo, *RSC advances*, 2018, **8**, 19157-19163.

[32] Y. Zeng, X. Zhang, Y. Meng, M. Yu, J. Yi, Y. Wu, X. Lu and Y. Tong, *Adv. Mater.*, 2017, **29**, 1700274.

[33] L.-P. Wang, N.-W. Li, T.-S. Wang, Y.-X. Yin, Y.-G. Guo and C.-R. Wang, *Electrochim. Acta*, 2017, **244**, 172-177.

[34] J. Zhao, J. Zhang, W. Yang, B. Chen, Z. Zhao, H. Qiu, S. Dong, X. Zhou, G. Cui and L. Chen, *Nano Energy*, 2019, **57**, 625-634.

[35] S. M. George, *Chem. Rev.*, 2009, **110**, 111-131.

[36] K. Zhao, C. Wang, Y. Yu, M. Yan, Q. Wei, P. He, Y. Dong, Z. Zhang, X. Wang and L. Mai, *Adv Mater Interfaces*, 2018, **5**, 1800848.

View Article Online
DOI: 10.1039/D0TA00748J

[37] A. C. Kozen, C.-F. Lin, A. J. Pearse, M. A. Schroeder, X. Han, L. Hu, S.-B. Lee, G. W. Rubloff and M. Noked, *ACS nano*, 2015, **9**, 5884-5892.

[38] E. Kazyak, K. N. Wood and N. P. Dasgupta, *Chem. Mater.*, 2015, **27**, 6457-6462.

[39] L. Chen, J. G. Connell, A. Nie, Z. Huang, K. R. Zavadil, K. C. Klavetter, Y. Yuan, S. Sharifi-Asl, R. Shahbazian-Yassar, J. A. Libera, A. U. Mane b and J. W. Elam, *J. Mater. Chem. A*, 2017, **5**, 12297-12309.

[40] Y. Zhao, L. V. Goncharova, A. Lushington, Q. Sun, H. Yadegari, B. Wang, W. Xiao, R. Li and X. Sun, *Adv. Mater*., 2017, **29**, 1606663.

[41] K. Wongrujipairoj, L. Poolnapol, A. Arpornwichanop, S. Suren and S. Kheawhom, *physica status solidi (b)*, 2017, **254**, 1600442.

[42] Y. Liu, Y. Qiao, W. Zhang, H. Wang, K. Chen, H. Zhu, Z. Li and Y. Huang, *J. Mater. Chem. A*, 2015, **3**, 7780-7785.

[43] M. Bou, J. Martin, T. Le Mogne and L. Vovelle, *Appl. Surf. Sci.*, 1991, **47**, 149-161.

[44] I. Iatsunskyi, M. Kempiński, M. Jancelewicz, K. Załęski, S. Jurga and V. Smyntyna, *Vacuum*, 2015, **113**, 52-58.

[45] G. Yang, D. Gao, J. Zhang, J. Zhang, Z. Shi and D. Xue, *The Journal of Physical Chemistry C*, 2011, **115**, 16814-16818.

[46] X. Shi, G. Xu, S. Liang, C. Li, S. Guo, X. Xie, X. Ma and J. Zhou, *ACS Sustainable Chemistry & Engineering*, 2019, **7**, 17737-17746.

[47] L. Dong, X. Ma, Y. Li, L. Zhao, W. Liu, J. Cheng, C. Xu, B. Li, Q.-H. Yang and F. Kang, *Energy Storage Mater*, 2018, **13**, 96-102.

[48] E. Diler, B. Lescop, S. Rioual, G. N. Vien, D. Thierry and B. Rouvellou, *Corros. Sci.*, 2014, **79**, 83-88.

[49] G. Deroubaix and P. Marcus, *Surf. Interface Anal.*, 1992, **18**, 39-46.

[50] G. Ballerini, K. Ogle and M.-G. Barthés-Labrousse, *Appl. Surf. Sci.*, 2007, **253**, 6860-6867.

[51] Y. Li, Y. Li, A. Pei, K. Yan, Y. Sun, C.-L. Wu, L.-M. Joubert, R. Chin, A. L. Koh and Y. Yu, *Science*, 2017, **358**, 506-510.

View Article Online
DOI: 10.1039/D0TA00748J

[52] W. Sun, F. Wang, S. Hou, C. Yang, X. Fan, Z. Ma, T. Gao, F. Han, R. Hu and M. Zhu, *J. Am. Chem. Soc.*, 2017, **139**, 9775-9778.

View Article Online
DOI: 10.1039/D0TA00748J

Table of Content

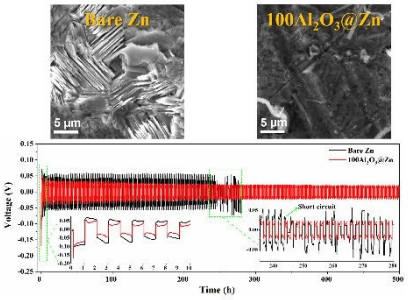

Nanoscale Al_2O_3 coating by atomic layer deposition technique enabled safe and dendrite-free Zn anode for rechargeable aqueous zinc-ion batteries.